ИЗВЕСТИЯ ВЫСШИХ УЧЕБНЫХ ЗАВЕДЕНИЙ.
Т 68 (4) Серия «**ХИМИЯ И ХИМИЧЕСКАЯ ТЕХНОЛОГИЯ**» 2025

V 68 (4) **ChemChemTech** 2025

DOI: 10.6060/ivkkt.20256804.7128

СИНТЕЗ И ФОТОКАТАЛИТИЧЕСКИЕ СВОЙСТВА ОКСИДА ЦЕРИЯ В РАЗЛОЖЕНИИ 2,4-D: ВЛИЯНИЕ МЕТОДОВ СИНТЕЗА

Нгуен Хоанг Хао, Фунг Тхи Лан, Нгуен Тхи Ким Занг, Као Хоанг Минь Чау, Нгуен Тхи Тху Ха

Нгуен Хоанг Хао (ORCID 0009-0000-5974-554X), Као Хоанг Минь Чау (ORCID 0009-0006-0136-385X)

Факультет химии, Педагогический колледж, Университет Винь, 182 Ле Зуан, Винь 460000, Вьетнам

Фунг Тхи Лан (ORCID 0000-0001-8509-6408), Нгуен Тхи Ким Занг (ORCID 0009-0007-8761-2200), Нгуен Тхи Тху Ха (ORCID 0000-0002-9979-2399)*

Факультет химии, Ханойский национальный педагогический университет, 136 Суан Тху, Каузяй, Ханой, Вьетнам
E-mail: ntt.ha@hnue.edu.vn*

Оксид церия (IV) (CeO_2) был синтезирован тремя различными методами: гидротермальным синтезом с водным растворителем и агентом OH-, гидротермальным синтезом с этаноловым растворителем и сольвотермальным синтезом со смесью органических растворителей. Синтезированные материалы были охарактеризованы с использованием ряда передовых техник, включая трансмиссионную электронную микроскопию (TEM), рентгеновскую дифракцию (XRD), рентгеновскую фотоэлектронную спектроскопию (XPS) и диффузно-отражательную спектроскопию в ультрафиолетовой и видимой областях (UV-Vis DRS). Фотокаталитическая активность синтезированных материалов CeO_2 была оценена путем разложения 2,4-дихлорфеноксиуксусной кислоты (2,4-D), распространенного гербицида. Результаты показали, что CeO_2, синтезированный гидротермальным методом с этаноловым растворителем, имел наименьший размер частиц, варьирующийся от 35 нм до 55 нм. Этот малый размер частиц является благоприятным для фотокаталитических применений, так как обеспечивает большую площадь поверхности для каталитических реакций. Следовательно, этот материал CeO_2 продемонстрировал хорошую фотокаталитическую активность, достигнув эффективности разложения до 54,14% для 2,4-D. Более того, кинетические исследования процесса разложения проводились с использованием модели псевдопервого порядка на основе механизма Лэнгмюра-Хиншельвуда. Полученные результаты показали, что константы скорости разложения 2,4-D на катализаторах CeO_2, синтезированных различными методами, были довольно схожими, что указывает на то, что метод синтеза в первую очередь влияет на размер частиц и поверхностные свойства, а не на внутреннюю каталитическую активность. Эти результаты подчеркивают важность оптимизации методов синтеза для повышения фотокаталитической эффективности материалов CeO_2 для экологической ремедиации.

Ключевые слова: CeO_2, фотокаталитическое разложение, 2,4-D, гидротермальный синтез, сольвотермальный синтез

Для цитирования:
Нгуен Хоанг Хао, Фунг Тхи Лан, Нгуен Тхи Ким Занг, Као Хоанг Минь Чау, Нгуен Тхи Тху Ха Синтез и фотокаталитические свойства оксида церия в разложении 2,4-D: влияние методов синтеза. *Изв. вузов. Химия и хим. технология*. 2025. Т. 68. Вып. 4. С. 25–32. DOI: 10.6060/ivkkt.20256804.7128.

For citation:
Nguyen Hoang Hao, Phung Thi Lan, Nguyen Thi Kim Giang, Cao Hoang Minh Chau, Nguyen Thi Thu Ha Synthesis and photocatalytic properties of cerium oxide in the degradation of 2,4-dichlorophenoxyacetic acid: influence of synthesis methods. *ChemChemTech [Izv. Vyssh. Uchebn. Zaved. Khim. Khim. Tekhnol.]*. 2025. V. 68. N 4. P. 25–32. DOI: 10.6060/ivkkt.20256804.7128.

SYNTHESIS AND PHOTOCATALYTIC PROPERTIES OF CERIUM OXIDE IN THE DEGRADATION OF 2,4-DICHLOROPHENOXYACETIC ACID: INFLUENCE OF SYNTHESIS METHODS

Nguyen Hoang Hao, Phung Thi Lan, Nguyen Thi Kim Giang, Cao Hoang Minh Chau, Nguyen Thi Thu Ha

Nguyen Hoang Hao (ORCID 0009-0000-5974-554X), Cao Hoang Minh Chau (ORCID 0009-0006-0136-385X)
Faculty of Chemistry, College of Education, Vinh University, 182 Le Duan, Vinh 460000, Vietnam

Phung Thi Lan (ORCID 0000-0001-8509-6408), Nguyen Thi Kim Giang (ORCID 0009-0007-8761-2200), Nguyen Thi Thu Ha (ORCID 0000-0002-9979-2399)*
Faculty of Chemistry, Hanoi National University of Education, 136 Xuan Thuy, Cau Giay, Ha Noi, Vietnam
E-mail: ntt.ha@hnue.edu.vn*

Ceria (CeO_2) was synthesized using three different methods: hydrothermal synthesis with water solvent and OH- agent, hydrothermal synthesis with ethanol solvent, and solvothermal synthesis. The synthesized materials were characterized using a range of advanced techniques, including Transmission Electron Microscopy (TEM), X-Ray Diffraction (XRD), X-Ray Photoelectron Spectroscopy (XPS), and UV-Visible Diffuse Reflectance Spectroscopy (UV-Vis DRS). The photocatalytic activity of the synthesized CeO_2 materials was evaluated through the degradation of 2,4-dichlorophenoxyacetic acid (2,4-D), a common herbicide. The results indicated that CeO_2 synthesized using the hydrothermal method with ethanol solvent had the smallest particle size, ranging from 35 to 55 nm. This small particle size is beneficial for photocatalytic applications as it provides a larger surface area for catalytic reactions. Consequently, this CeO_2 material exhibited excellent photocatalytic activity, achieving a degradation efficiency of up to 54.14% for 2,4-D. Kinetic studies of the degradation process were conducted using a pseudo-first-order reaction model based on the Langmuir-Hinshelwood mechanism. These studies revealed that the degradation rate constants of 2,4-D on CeO_2 catalysts synthesized by the different methods were quite similar, suggesting that the synthesis method primarily influences the particle size and surface properties rather than the intrinsic catalytic activity. These findings highlight the importance of optimizing synthesis methods to enhance the photocatalytic efficiency of CeO_2 materials for environmental remediation applications.

Keywords: CeO_2, photocatalytic degradation, 2,4-D, hydrothermal synthesis, solvothermal synthesis

INTRODUCTION

CeO_2, or cerium oxide, is a versatile semiconductor with numerous practical applications across various fields. One of the most significant and rapidly growing applications of CeO_2 is its use as a photocatalyst for the degradation of various pollutants in wastewater treatment [1]. CeO_2's high oxygen storage capacity and unique redox properties, which enable it to easily switch between Ce^{3+} and Ce^{4+} oxidation states, make it an excellent material for photocatalytic applications [2]. Additionally, the high thermal stability, hardness, and remarkable redox behavior [3, 4] allow CeO_2 to efficiently facilitate the breakdown of organic pollutants under light irradiation, making it an invaluable material for environmental remediation.

CeO_2 has been successfully synthesized through various methods solvothermal methods [5], precipitation methods [6], combustion synthesis [7], sol-gel methods [8], etc., each offering distinct advantages and challenges tailored to specific applications and material requirements, such as: Among these methods, solvothermal synthesis is favored for producing CeO_2 nanoparticles due to its capability to control particle size, morphology, and ensure high purity under specific conditions of solvents and controlled temperature and pressure. The choice of solvent, like water or ethanol, influences CeO_2's dispersibility, surface area, and crystallinity, impacting its catalytic performance and suitability for different technological uses [9]. Understanding these solvent-dependent effects is crucial for tailoring CeO_2 synthesis to achieve desired material characteristics and enhance its functional properties in diverse applications.

In this study, we present the synthesis of CeO_2 nanoparticles through three distinct methods: hydrothermal synthesis utilizing a water solvent and OH- agent, hydrothermal synthesis employing an ethanol solvent, and solvothermal synthesis with a blend of organic solvents. The resulting nanoparticles were metic-

ulously characterized using Transmission Electron Microscopy (TEM), X-Ray Diffraction (XRD), X-Ray Photoelectron Spectroscopy (XPS), and UV-Visible Diffuse Reflectance Spectroscopy (UV-Vis DRS). We further investigated the photocatalytic properties of these materials by examining the degradation of 2,4-dichlorophenoxyacetic acid (2,4-D) under illumination from a 250 W xenon lamp. This comprehensive analysis aims to elucidate the relationship between synthesis methods and the structures and photocatalytic efficiency of CeO_2 nanoparticles.

EXPERIMENTS

Chemicals

$Ce(NO_3)_3 \cdot 6H_2O$, toluene, oleic acid, ethanol, ammonia, and tert-butylamine were purchased from Sigma-Aldrich and used directly without any additional purification steps.

Material Synthesis

Synthesis by Hydrothermal Method Using Water Solvent and OH^- Agent

1.5 g of $Ce(NO_3)_3 \cdot 6H_2O$ was dissolved in 50 ml of deionized water in a glass beaker. Ammonia, serving as the OH^- agent, was slowly added to the beaker to adjust the pH of the solution while stirring. The mixture was then transferred to a Teflon-lined autoclave, which was placed inside a stainless steel vessel. The hydrothermal process was conducted at various temperatures for 24 h. After cooling to room temperature, the precipitated particles were centrifuged, washed multiple times with distilled water, and dried at 100 °C for 24 h. The resulting solid product was labeled as CeO_2-a.

Synthesis by Hydrothermal Method Using Ethanol Solvent

1.5 g of $Ce(NO_3)_3 \cdot 6H_2O$ was dissolved in 50 ml of ethanol and stirred until a stable suspension was formed. The suspension was transferred to a Teflon-lined autoclave, which was placed inside a stainless steel vessel. The hydrothermal process was conducted at various temperatures for 24 h. After cooling to room temperature, the precipitated particles were centrifuged, washed multiple times with distilled ethanol, and dried at 80 °C for 24 h. The resulting solid product was labeled as CeO_2-b.

Synthesis by Solvothermal Method Using Mixture of Organic Solvents

1.5 g of $Ce(NO_3)_3 \cdot 6H_2O$ was dissolved in 80 ml of deionized water. To the solution, 2 ml of tert-butylamine, 80 ml of toluene, and 10 ml of oleic acid were added. The mixture was transferred to a Teflon-lined autoclave, which was placed inside a stainless steel vessel. The solvothermal process was conducted at 160-200 °C for 24 h. After the reaction, the mixture was separated to collect the upper toluene phase. CeO_2 nanoparticles were isolated by adding 100 ml of ethanol to the mixture, followed by centrifugation. The solid obtained after centrifugation was dried at 80 °C and labeled as CeO_2-c.

Material Characterization

Transmission Electron Microscopy (TEM) was performed using a JEM 1400 microscope from JEOL. UV-Visible Diffuse Reflectance Spectroscopy (UV-Vis DRS) to evaluate the light absorption of the materials was conducted on a Shimadzu UV-2600 instrument. X-Ray Diffraction (XRD) to assess the crystalline phases was performed on a Bruker D8 Advance diffractometer with a Cu-Kα radiation source (wavelength 0.15418 nm). XPS measurements were conducted using a Nexsa XPS system (ThermoFisher Scientific) with monochromatic Al Kα radiation (hν = = 1486.6 eV). Calibration was based on the binding energy of the C1s peak at approximately 284.8 eV. Spectral analysis was performed using the XPSPEAK41 software.

RESULTS AND DISCUSSIONS

Material Characterization

CeO_2 samples synthesized by three different methods were examined at temperatures of 160, 180, and 200 °C to study the changes in the size of the resulting nanoparticles. Transmission Electron Microscopy (TEM) images (Fig. 1) were used to investigate the morphology and particle size of the materials.

The TEM images from Fig. 1 reveal distinct characteristics of CeO_2 samples synthesized using three different methods. In the hydrothermal method with water solvent (CeO_2-a) and OH^- agent, unevenly crystalline particles are observed. At 160 °C (Fig. 1A), particle sizes range from 30 nm to 150 nm, with prominent larger clusters. At higher crystallization temperatures of 180 °C (Fig. 1B) and 200 °C (Fig. 1C), particles exhibit hexagonal structures but significantly increase in size, ranging from 200-300 nm.

TEM images of samples synthesized via the hydrothermal method with ethanol solvent (CeO_2-b) show less defined particle clusters at 160 °C. As the temperature increases to 180 °C (Fig. 1E), clearer particle clusters ranging from 50-90 nm emerge. At 200 °C, particle sizes exceed 100 nm with more distinct clusters.

For the solvothermal method (CeO_2-c), poor definition of particle clusters is noted at 160 °C, improving at 180 °C with particle sizes ranging from 7-8 nm. A further increase to 200 °C shows minimal change in particle size, indicating a 2D cluster structure development.

For catalytic applications, CeO_2 samples synthesized at 180 °C underwent annealing at 600 °C to enhance their structural stability and catalytic activity. The TEM images in Fig. 2 depict the morphology and crystalline characteristics of the annealed CeO_2 nanoparticles, providing insights into their suitability and effectiveness for catalytic processes.

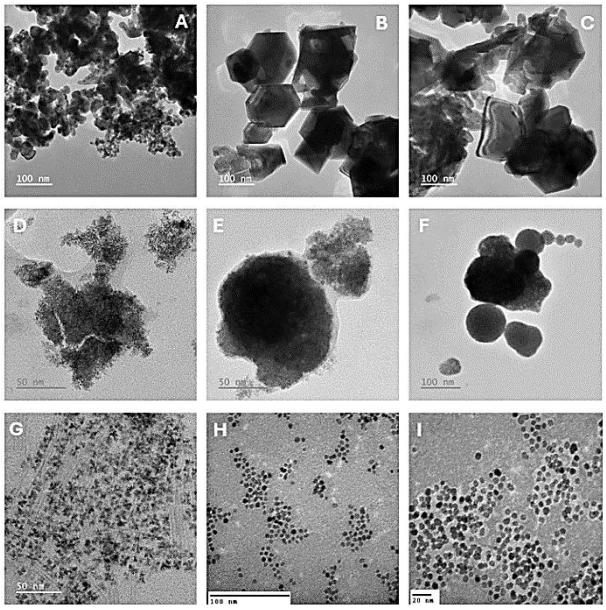

Fig. 1. TEM images of CeO_2 samples: CeO_2-a at 160°C (A), 180°C (B), and 200°C (C); CeO_2-b at 160°C (D), 180°C (E), and 200°C (F); and CeO_2-c at 160°C (G), 180°C (H), and 200°C (I)

Рис. 1. ТЕМ изображения образцов CeO_2: CeO_2-a при 160°C (A), 180°C (B) и 200°C (C); CeO2-b при 160°C (D), 180°C (E) и 200°C (F); и CeO_2-c при 160°C (G), 180°C (H) и 200°C (I)

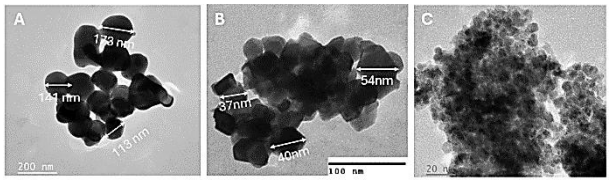

Fig. 2. TEM images of CeO_2-a-600, CeO_2-b-600, and CeO_2-c-600 samples

Рис. 2. ТЕМ-изображения образцов CeO_2-a-600, CeO_2-b-600 и CeO_2-c-600

From the TEM images, it is clear that after annealing at 600 °C, the hydrothermal method with water solvent (sample CeO_2-a-600, Fig. 2A) produces relatively large particles, ranging from 110-170 nm. In contrast, the hydrothermal method with ethanol solvent (sample CeO_2-b-600, Fig. 2B) yields particles with sizes ranging from 35-55 nm. The solvothermal method (sample CeO_2-c-600, Fig. 2C) results in highly uniform particles, approximately 7-8 nm in size. This demonstrates that the hydrothermal method with ethanol solvent and the solvothermal method produce smaller and more uniform CeO_2 particle clusters compared to the hydrothermal method with water solvent.

To gain a deeper understanding of the crystal structures of the materials, the XRD spectra of CeO_2 samples synthesized at 180 °C by the three methods and annealed at 600 °C are presented in Fig. 3.

The XRD results from Fig. 3 indicate that the XRD patterns of CeO_2-a-600, CeO_2-b-600, and CeO_2-c-600 all display characteristic peaks of CeO_2 crystals with a fluorite structure (JCPDS 34-0349) at 2-theta values of: 28.5 (111), 33.08 (200), 47.47 (220), 56.33 (311), 59.08 (222), 69.40 (400), 76.69 (331), and 79.06 (420). In the CeO_2-a-600 and CeO_2-b-600 samples, the peaks are intense, sharp, and well-defined, while in the CeO_2-c-600 sample, the peaks are lower in intensity and broader. This indicates that the crystal structure of CeO_2 in the hydrothermal method samples is better defined compared to the solvothermal method.

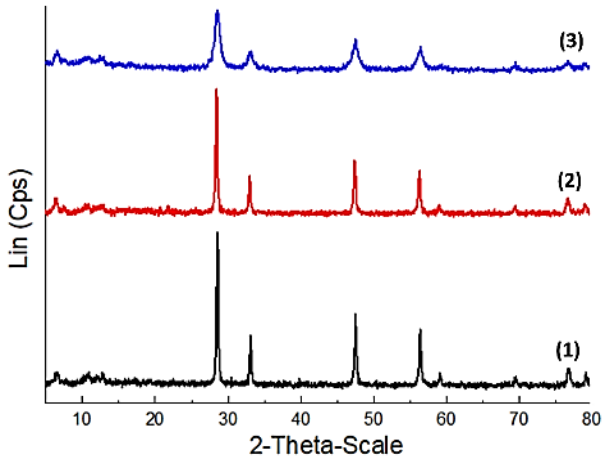

Fig. 3. XRD spectra of CeO_2 samples synthesized by three methods and annealed at 600°C: (1) – CeO_2–a; (2) – CeO_2–b; (1) – CeO_2–c

Рис. 3. Рентгеновские дифрактограммы (XRD) образцов CeO_2, интезированных тремя методами и отожженных при 600°C: (1) – CeO_2–a; (2) – CeO_2–b; (1) – CeO_2–c

XPS analysis was conducted to determine the oxidation states and elemental composition of the materials. This measurement was performed on a representative sample, CeO_2-b-600. The XPS analysis results are presented in Fig. 4. To analyze the relative content of Ce(III) on the material's surface, XPS Ce 3d spectra were used, based on the spin-orbit components $3d_{5/2}$ and $3d_{3/2}$ of cerium ions [10, 11]. The XPS Ce 3d analysis results are shown in Figure 4, with peaks at 880.2, 885.0, 899.5, and 903.5 eV corresponding to Ce^{3+} states, while peaks at 882.1, 888.1, 898.0, 900.9, 906.4, and 916.4 eV correspond to Ce^{4+} states [11]. The relative concentration of Ce(III) was calculated from the integrated areas of the deconvoluted peaks using equation (1):

$$[Ce^{3+}] = \frac{A_{v_o}+A_{v'}+A_{u_o}+A_{u'}}{A_{v_o}+A_{v'}+A_{u_o}+A_{u'}+A_{v}+A_{v''}+A_{v'''}+A_{u}+A_{u'}+A_{u''}+A_{u'''}} \quad (1)$$

From the analysis of the Ce 3d spectrum, the concentration of Ce(III) in the CeO_2-b-600 sample was determined to be 28.33%. This result is relatively high compared to some previously reported CeO_2 samples [10, 12]. The presence of a significant amount of Ce(III) can create oxygen vacancies in the crystal structure. These oxygen vacancies suggest that the CeO_2 material may exhibit good photocatalytic activity.

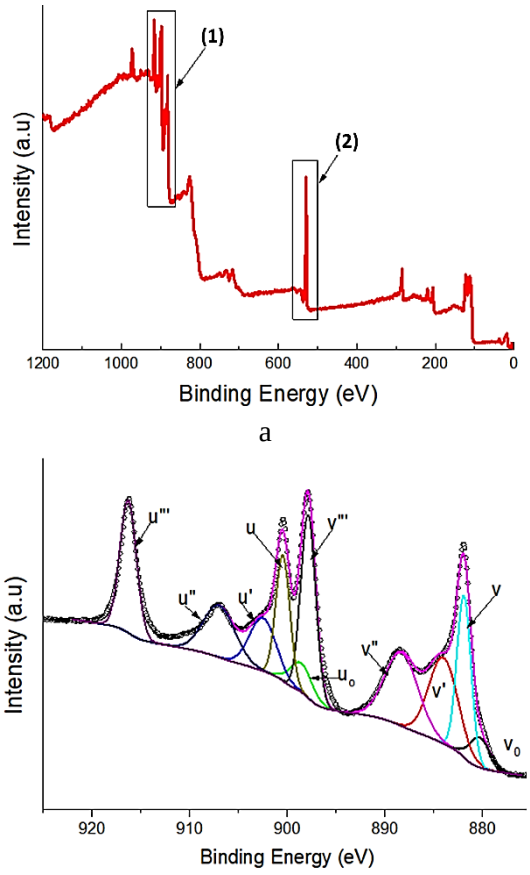

Fig. 4. XPS survey of CeO_2-b-600 (a): (1) – Ce3d; (2) – O1s; XPS Ce3d spectra of CeO_2-b (b): Ce^{4+}– v, v'', v''', u, u'', u''' ; Ce^{3+}–v_o, v', u_o, u'; v: $3d_{5/2}$; u: $3d_{3/2}$

Рис. 4. Обзорный спектр XPS образца CeO_2-b-600 (a): (1) – Ce3d; (2) – O1s; спектры XPS Ce3d образца CeO_2-b-600 (b): Ce^{4+}– v, v'', v''', u, u'', u''' ; Ce^{3+}– v_o, v', u_o, u'; v: $3d_{5/2}$; u: $3d_{3/2}$

To further investigate the optical absorption capabilities of the synthesized CeO_2 samples, CeO_2-b-600 was chosen for UV-Vis-DRS analysis. The results are depicted in Fig. 5.

It can be observed that the UV-vis spectrum of CeO_2-b-600 (Fig. 5a) exhibits a broad peak in the UV region around 345 nm, with the shoulder extending beyond 400 nm, indicating its ability to absorb across the visible region. The bandgap energy (E_g) is determined based on the relationship between the absorption coefficient (α) and E_g according to the Kubelka-Munk theory (equation (2) [13]):

$$(\alpha.h\upsilon)^n = A(h\upsilon - Eg) \quad (2)$$

where, α is the absorption coefficient, E_g is the bandgap, A is a constant, and hυ is the photon energy. The value of E_g is extrapolated from the linear portion of the graph on (Fig. 5b), revealing E_g of CeO_2 to be 3.00 eV, which is consistent with the previous reported E_g values [14].

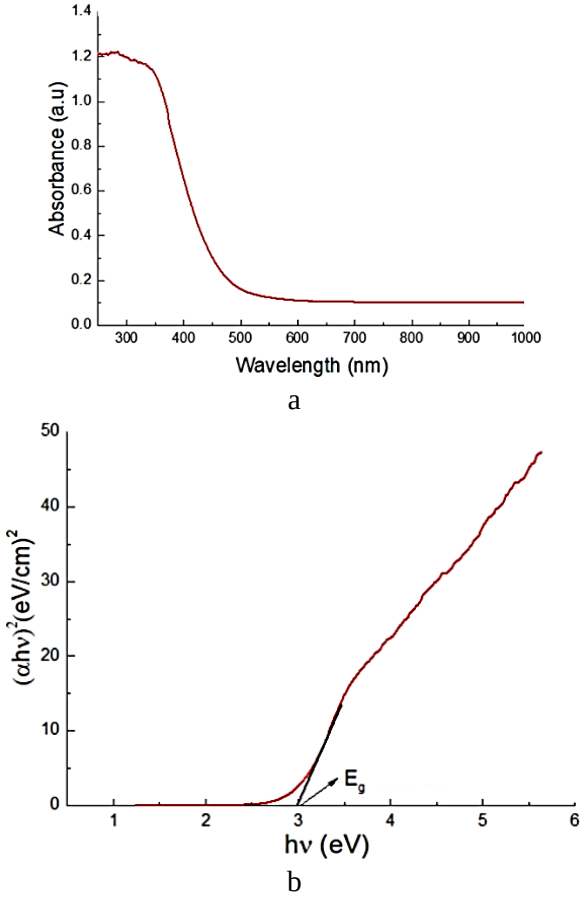

Fig. 5. UV-Vis spectrum (a) and Tauc plot (b) of the CeO_2-b-600 sample

Рис. 5. УФ-ВИС спектр (a) и Таук график (b) образца CeO_2-b-600

Photocatalytic activity of CeO_2 in degradation of 2,4-D

Photocatalytic activity of the materials

To evaluate the photocatalytic activity of the material, we conducted experiments where 0.075 g of catalyst was added to 150 ml of 2,4-D solution initially at a concentration of 40 mg/L. The experiments were carried out in dark conditions for 60 min to assess the material's adsorption capacity. Subsequently, the samples were exposed to irradiation under a 250W Xenon lamp. Throughout the experiment, samples were extracted

every 30 min to measure the 2,4-D concentration using a UV-Vis spectrophotometer at a wavelength of 283 nm. Additionally, a calibration curve was generated to quantify the concentration of 2,4-D (Supplementary Information).

The photodegradation of 2,4-D was conducted using all three CeO_2-a-600, CeO_2-b-600, and CeO_2-c-600 material samples. The obtained results (Fig. 6A) indicate that CeO_2 exhibits minimal capacity for adsorbing 2,4-D. After 60 min of stirring in darkness, there was a negligible decrease in the concentration of 2,4-D (approximately 2-3%). Regarding photocatalysis, all three CeO_2 samples (a, b, and c) generally demonstrate effective 2,4-D degradation capabilities. Upon closer examination, CeO_2-a-600 and CeO_2-b-600 show similar abilities in 2,4-D degradation, while CeO_2-c-600 exhibits slightly lower but not significantly different performance.

The conversion efficiencies of the samples are calculated and presented in Fig. 6B. After 240 min of irradiation, CeO_2-a-600, CeO_2-b-600, and CeO_2-c-600 achieve conversion efficiencies of 53.36%, 54.14%, and 49.70% for 2,4-D, respectively.

To assess whether the selected material exhibits sufficient effectiveness, we reviewed and organized key findings from previous studies, as summarized in Table 1.

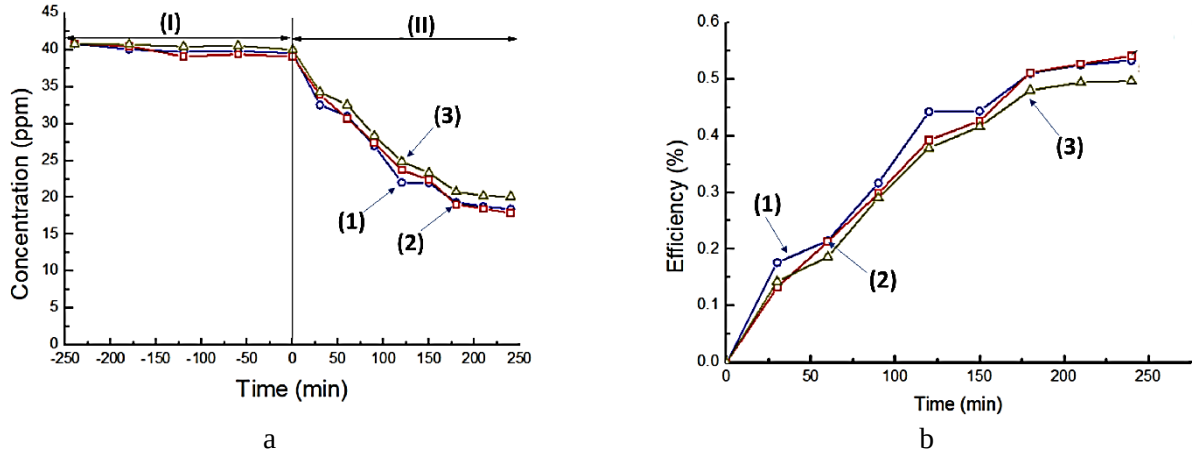

a b

Fig. 6. (a): Photocatalytic degradation reaction of 2,4-D using CeO_2-a-600 (1), CeO_2-b-600 (2), and CeO_2-c-600 materials (3); (I) – dark; (II) – light; (b): conversion efficiencies of the samples: CeO_2-a-600 (1), CeO_2-b-600 (2), and CeO_2-c-600 materials (3)

Рис. 6. (a): Фотокаталитическая реакция деградации 2,4-D для CeO_2-a-600 (1), CeO_2-b-600 (2) и CeO_2-c-600 (3) образцов; (I) – в темноте; (II) – при освещении; (b): эффективность преобразования 2,4-D для CeO_2-a-600 (1), CeO_2-b-600 (2) и CeO_2-c-600 (3) образцов

Table 1

Comparison of photocatalytic degradation efficiencies of 2,4-D by various catalysts

Таблица 1. **Сравнение эффективности фотокаталитического разложения 2,4-D различными катализаторами**

Catalyst	Catalyst Amount	RhB Concentration	Light Source	Illumination Time (min)	Degradation Efficiency (%)	Reference
3%Pt/TiO_2	120 mg	800 mL (20mg/L) = 16 mg	mercury-lamp (400 W)	90	54.64	[15]
1%N-TiO_2-SG	100 mg	100 mL (40 mg/L) = 4 mg	visible light (250W)	180	55.21	[16]
Fe_2O_3/CeO_2/Ag	20 mg	250 mL (30 mg/L) = 7.5 mg	UV lamp	150	75.70	[17]
TiO_2-clinoptilolite	0.4 g/L	5 mg/L	UV lamp	25	65.00	[18]
ZnO/γ-Fe_2O_3/UVA	0.2 g/L	20 mg/L	UV lamp	240	52.50	[19]
CeO_2 -b-600	75 mg	150 mL (40 mg/L) = 3 mg	Xenon lamp (250W)	240	54.14	This work

The results in Table 1 reveal that the CeO_2-b-600 sample demonstrates commendable photocatalytic performance compared to several previously studied materials. A key advantage of the material developed in this study lies in its simple synthesis process and high degradation efficiency at the native pH of the 2,4-D solution, eliminating the need for additional chemicals to adjust the solution's pH. These attributes underscore the significant potential of the synthesized CeO_2 material for photocatalytic applications, positioning it as a promising candidate for further research.

Kinetics of the photocatalytic degradation process of 2,4-D on synthesized materials

Previous studies have indicated that photocatalytic degradation reactions can be approximated by pseudo-first-order kinetics using the Langmuir-Hinshelwood model [20-23]:

$$r = -\frac{dC}{dt} = k\,\frac{K_a C}{1+K_a C} \qquad (3.a)$$

At low concentrations of reactants, the equation can be simplified to:

$$r = -\frac{dC}{dt} \approx k\cdot K_a C = k_{ap} C \qquad (3.b)$$

The integrated form resembles first-order kinetics:

$$ln\frac{C_0}{C_t} = k_{ap} t \qquad (3.c)$$

Experimental data were analyzed for pseudo-first-order kinetics. The results are presented in Fig. 7.

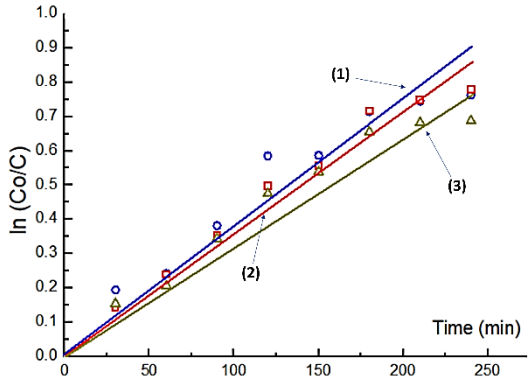

Fig. 7. Apparent first-order kinetics of the photocatalytic degradation reaction of 2,4-D (C_0 = 40 ppm, 240 min of irradiation) for the samples: CeO_2-a-600 (1), CeO_2-b-600 (2), and CeO_2-c-600 materials (3)
Рис. 7. Кажущаяся кинетика первого порядка реакции фотокаталитической деградации 2,4-D (C_0 = 40 ppm, 240 мин облучения) для CeO_2-a-600 (1), CeO_2-b-600 (2) и CeO_2-c-600 (3) образцов

The kinetic parameters of the photocatalytic degradation process of 2,4-D are summarized in Table 2.

Table 2

Apparent rate constants of the photocatalytic degradation of 2,4-D on the catalyst samples

***Таблица 2*. Кажущиеся константы скорости фотокаталитической деградации 2,4-D на образцах катализатора**

Sample	CeO_2-a-600	CeO_2-b-600	CeO_2-c-600
$k_{ap}(min^{-1})$	0.0037	0.0036	0.0033
R^2	0.9844	0.9922	0.9864

The rate constants for the degradation of 2,4-D on CeO_2-a-600 and CeO_2-b-600 catalysts are observed to be similar and slightly higher than those on CeO_2-c-600 catalyst. Based on the obtained results, the following observations can be made: i) CeO_2 demonstrates photocatalytic activity in the degradation of 2,4-D; ii) under the established experimental conditions, photocatalytic activity appears independent of the synthesis method; iii) The photocatalytic efficiency of CeO_2 is more pronounced in the UV region compared to the visible region, attributed to its bandgap energy of 3.2 eV determined by UV-vis DRS spectroscopy. Consequently, the conversion efficiency of 2,4-D remains modest, achieving just over 50% for all three synthesized samples. To enhance the optical properties of CeO_2, ongoing investigations include modifications such as doping with various non-metals or combining it with other semiconductors, with results to be detailed in forthcoming publications.

CONCLUSIONS

CeO_2 nanoparticle were successfully synthesized using three methods: hydrothermal synthesis with water, hydrothermal synthesis with ethanol, and solvothermal synthesis with mixture of organic solvents. The findings demonstrated that the hydrothermal synthesis with ethanol yielded samples with significantly higher fabrication efficiency. TEM images indicated particle sizes ranging from 35 to 55 nm. XRD, XPS, and UV-Vis analyses collectively confirmed the synthesized CeO_2 material exhibited robust photocatalytic activity in degrading 2,4-D, achieving an efficiency of 54.14%. While the catalytic activity of CeO_2 showed minimal dependence on the preparation method, the ethanol hydrothermal method produced particles with well-defined crystal structures. Moreover, this method utilized simpler chemicals, exhibited superior particle fabrication efficiency compared to solvothermal methods, and was more cost-effective, thus presenting favorable attributes for catalytic material fabrication.

ACKNOWLEDGEMENT

This research is funded by Vietnam Ministry of Education and Training under grant number B2022-TDV-06.

The authors declare the absence of a conflict of interest warranting disclosure in this article.

Данное исследование финансируется Министерством образования и профессиональной подготовки Вьетнама в рамках гранта номер B2022-TDV-06.

Авторы заявляют об отсутствии конфликта интересов, требующего раскрытия в данной статье.

REFERENCES
ЛИТЕРАТУРА

1. **Fauzi A., Jalil A., Hassan N., Aziz F., Azami, Hussain I., Saravanan R., Vo D.V.** A critical review on relationship of CeO_2-based photocatalyst towards mechanistic degradation of organic pollutant. *Chemosphere*. 2022. V. 286. P. 131651. DOI: 10.1016/j.chemosphere.2021.131651.
2. **Galyamin D., Ernst L.M., Fitó-Parera A., Mira-Vidal G., Bastús N.G., Sabaté N., Puntes V.** Nanoceria dissolution at acidic pH by breaking off the catalytic loop. *Nanoscale*. 2022. V. 14. N 38. P. 14223–14230. DOI: 10.1039/d2nr03586c.
3. **Rajendran P., Muthuraj A., Rajagounder N.E.** Review on CeO_2-Based Corrosion Coatings. *Trans. Indian Ceram. Soc.* 2022. V. 81, N 4. P. 158–174. DOI: 10.1080/0371750x.2022.2149623.
4. **Черкасова Е.В., Черкасова Т.Г.** Физико-химические характеристики материалов на основе лантаноидов цериевой группы и хрома. *Изв. вузов. Химия и хим. технология*. 2022. Т. 65. Вып. 10. С. 54-60. **Cherkasova E.V., Cherkasova T.G.** Physico-chemical characteristics of materials based on cerium and chromium lanthanoides. *ChemChemTech [Izv. Vyssh. Uchebn. Zaved. Khim. Khim. Tekhnol.]*. 2022. V. 65. N 10. P. 54-60 (in Russian). DOI: 10.6060/ivkkt.20226510.6643.
5. **Sun C., Li H., Zhang H., Wang Z., Chen L.** Controlled synthesis of CeO_2 nanorods by a solvothermal method. *Nanotechnology*. 2005. V. 16. N 9. P. 1454–1463. DOI: 10.1088/0957-4484/16/9/006.
6. **Shlapa Y., Solopan S., Sarnatskaya V., Siposova K., Garcarova I., Veltruska K., Timashkov I., Lykhova O., Kolesnik D., Musatov A., Nikolaev V., Belous A.** Cerium dioxide nanoparticles synthesized via precipitation at constant pH: Synthesis, physical-chemical and antioxidant properties. *Colloids Surf. B Biointerfaces*. 2022. V. 220. P. 112960. DOI: 10.1016/j.colsurfb.2022.112960ю
7. **Mokkelbost T., Kaus I., Grande T., Einarsrud M.A.** Combustion Synthesis and Characterization of Nanocrystalline CeO_2-Based Powders. *Chem. Mater*. 2004. V. 16. N 25. P. 5489–5494. DOI: 10.1021/cm048583p.
8. **Fudala A.S., Salih W.M., Alkazaz F.F.** Synthesis different sizes of cerium oxide CeO_2 nanoparticles by using different concentrations of precursor via sol–gel method. *Mater. Today Proc.* 2022. V. 49. P. 2786–2792. DOI: 10.1016/j.matpr.2021.09.452.
9. **Walton R.I.** Solvothermal synthesis of cerium oxides. *Prog. Cryst. Growth Charact. Mater.* 2011. V. 57. N 4. P. 93–108. DOI: 10.1016/j.pcrysgrow.2011.10.002.
10. **Zang C., Zhang X., Hu S., Chen F.** The role of exposed facets in the Fenton-like reactivity of CeO_2 nanocrystal to the Orange II. *Appl. Catal. B: Environ.* 2017. V. 216. P. 106–113. DOI: 10.1016/j.apcatb.2017.05.068.
11. **Tsunekawa S., Fukuda T., Kasuya A.** X-ray photoelectron spectroscopy of monodisperse CeO_{2-x} nanoparticles. *Surf. Sci.* 2000. V. 457. N 3. P. L437–L440. DOI: 10.1016/s0039-6028(00)00470-2.
12. **Cai W., Chen F., Shen X., Chen L., Zhang J.** Enhanced catalytic degradation of AO7 in the CeO_2–H_2O_2 system with Fe^{3+} doping. *Appl. Catal. B: Environ.* 2010. V. 101. N 1–2. P. 160–168. DOI: 10.1016/j.apcatb.2010.09.031.
13. **Yang L., Kruse B.** Revised Kubelka–Munk theory I Theory and application. *J. Opt. Soc. Am. A Opt. Image Sci. Vis.* 2004. V. 21. N 10. P. 1933. DOI: 10.1364/josaa.21.001933.
14. **Ahmed S.H., Bakiro M., Aljasmi F.I.A., Albreiki A.M.O., Bayane S., Alzamly A.** Investigation of the band gap and photocatalytic properties of CeO_2/rGO composites. *Mol. Catal.* 2020. V. 486. P. 110874. DOI: 10.1016/j.mcat.2020.110874.
15. **Abdennouri M., Elhalil A., Farnane M., Tounsadi H., Mahjoubi F.Z., Elmoubarki R., Sadiq M., Khamar L., Galadi A., Baalala M., Bensitel M., El hafiane Y., Smith A., Barka N.** Photocatalytic degradation of 2,4-D and 2,4-DP herbicides on Pt/TiO_2 nanoparticles. *J. Saudi Chem. Soc.* 2015. V. 19. P. 485-493. DOI: 10.1016/j.jscs.2015.06.007.
16. **Del Ángel-Sanchez K., Vázquez-Cuchillo O., Aguilar-Elguezabal A., Cruz-López A., Herrera-Gómez A.** Photocatalytic degradation of 2,4-dichlorophenoxyacetic acid under visible light: Effect of synthesis route. *Mater. Chem. Phys.* 2013. V. 139. P. 423-430. DOI: 10.1016/j.matchemphys.2013.01.009.
17. **Karimipour Z., Yengejeh R.J., Haghighatzadeh A., Mohammadi M.K., Rouzbahani M.M.** Photocatalytic Degradation of 2,4-Dichlorophenoxy acetic Acid Using Fe_2O_3/CeO_2/Ag Composite Nanoparticles under Ultraviolet Irradiation. *J. Environ. Health Res.* 2021. V. 9. P. 191-200. DOI: 10.32598/JAEHR.9.3.1190.
18. **Mehrabadi Z., Faghihian H.** Clinoptilolite modified with TiO_2 for simultaneous elimination of two herbicides; 2,4-D and MCPA by UV and sunlight-assisted photocatalytic degradation. *Mater. Res. Bull.* 2019. V. 119. P. 110569. DOI: 10.1016/j.materresbull.2019.110569.
19. **Lee K.M., Abdullah A.H.** Synthesis and characterization of zinc oxide/maghemite nanocomposites: Influence of heat treatment on photocatalytic degradation of 2,4-dichlorophenoxyacetic acid. *Mater. Sci. Semicond. Process.* 2015. V. 30. P. 298-306. DOI: 10.1016/j.mssp.2014.10.017.
20. **Bian X., Chen J., Ji R.** Degradation of 2,4-Dichlorophenoxyacetic Acid (2,4-D) by Novel Photocatalytic Material of Tourmaline-Coated TiO_2 Nanoparticles: Kinetic Study and Model. *Materials*. 2013. V. 6. N 4. P. 1530–1542. DOI: 10.3390/ma6041530.
21. **Овчинников Н.Л., Виноградов Н.М., Гордина Н.Е., Бутман М.Ф.** Применение активирующих воздействий в получении TiO_2-пилларного монтмориллонита с улучшенными фотокаталитическими свойствами. *Изв. вузов. Химия и хим. технология*. 2023. Т. 66. Вып. 5. С. 59-71 **Ovchinnikov N.L., Vinogradov N.M., Gordina N.E., Butman M.F.** Application of activating influences in obtaining TiO_2-pillared montmorillonitewith improved photocatalytic properties. *ChemChemTech [Izv. Vyssh. Uchebn. Zaved. Khim. Khim. Tekhnol.]*. 2023. V. 66. N 5. P. 59-71 (in Russian). DOI: 10.6060/ivkkt.20236605.6798.
22. **Lan P.T., Hao N.H., Cam L.M.** Study on the Synthesis and Photocatalytic Performance of Modified TiO_2 Supported by g-C_3N_4 in the Degradation of 2,4-Dichlorophenoxyacetic Acid. *Chem. Select.* 2024. V. 9. N 12. e202305026. DOI: 10.1002/slct.202305026.
23. **Lan P.T., Hao N.H., Hieu N.T., Ha N.T.T., Brown C.T., Cam L.M.** Graphitic carbon nitride supported silver nanoparticles (AgNPs/g-C_3N_4): synthesis and photocatalytic behavior in the degradation of 2,4-dichlorophenoxyacetic acid. *RSC Adv.* 2024. V. 14. N 27. P. 19014–19028. DOI: 10.1039/d4ra02658f.

Поступила в редакцию (Received) 20.08.2024
Принята к опубликованию (Accepted) 02.12.2024